Visualization of human T lymphocyte-mediated eradication of cancer cells in vivo

Xingkang He[a,b], Xin Yin[a,c], Jing Wu[a], Stina L. Wickström[d], Yanhong Duo[a], Qiqiao Du[a,e], Shuhang Qin[a,e], Shuzhong Yao[e], Xu Jing[a], Kayoko Hosaka[a], Jieyu Wu[a], Lasse D. Jensen[f], Andreas Lundqvist[d], Alexander I. Salter[g], Lars Bräutigam[h], Wei Tao[i], Yuguo Chen[j], Rolf Kiessling[d], and Yihai Cao[a,1]

[a]Department of Microbiology, Tumor, and Cell Biology, Karolinska Institutet, 171 65 Stockholm, Sweden; [b]Department of Gastroenterology, Sir Run Run Shaw Hospital, Zhejiang University School of Medicine, 310058 Hangzhou, Zhejiang, China; [c]Department of Radiation Oncology, The First Affiliated Hospital, Zhejiang University School of Medicine, 310003 Hangzhou, Zhejiang, China; [d]Department of Oncology and Pathology, Karolinska Institutet, 171 77 Stockholm, Sweden; [e]Department of Obstetrics and Gynecology, The First Affiliated Hospital, Sun Yat-sen University, 510080 Guangzhou, China; [f]Division of Cardiovascular Medicine, Department of Medical and Health Sciences, Linkoping University, 581 83 Linkoping, Sweden; [g]Center and Department of Medicine, Fred Hutchinson Cancer Research Center, Seattle, WA 98109; [h]Comparative Medicine, Karolinska Institutet, SE-17177 Stockholm, Sweden; [i]Center for Nanomedicine and Department of Anesthesiology, Brigham and Women's Hospital, Harvard Medical School, Boston, MA 02115; and [j]Department of Emergency Medicine, Shandong Provincial Clinical Research Center for Emergency and Critical Care Medicine, Institute of Emergency and Critical Care Medicine of Shandong University, Qilu Hospital of Shandong University, 250012 Jinan, Shandong, China

Edited by Robert Langer, Massachusetts Institute of Technology, Cambridge, MA, and approved July 27, 2020 (received for review May 14, 2020)

Lymphocyte-based immunotherapy has emerged as a breakthrough in cancer therapy for both hematologic and solid malignancies. In a subpopulation of cancer patients, this powerful therapeutic modality converts malignancy to clinically manageable disease. However, the T cell- and chimeric antigen receptor T (CAR-T) cell-mediated antimetastatic activity, especially their impacts on microscopic metastatic lesions, has not yet been investigated. Here we report a living zebrafish model that allows us to visualize the metastatic cancer cell killing effect by tumor- infiltrating lymphocytes (TILs) and CAR-T cells in vivo at the single-cell level. In a freshly isolated primary human melanoma, specific TILs effectively eliminated metastatic cancer cells in the living body. This potent metastasis-eradicating effect was validated using a human lymphoma model with CAR-T cells. Furthermore, cancer-associated fibroblasts protected metastatic cancer cells from T cell-mediated killing. Our data provide an in vivo platform to validate antimetastatic effects by human T cell-mediated immunotherapy. This unique technology may serve as a precision medicine platform for assessing anticancer effects of cellular immunotherapy in vivo before administration to human cancer patients.

cancer | metastasis | lymphocyte | zebrafish | cancer therapy

Cancer immunotherapy is emerging as a curative therapy for a subpopulation of cancer patients (1–10). This therapeutic modality is based on boosting either the patient's own immune system to eliminate cancer cells or genetically propagating cancer-recognizing T cells in vitro and administering them back to cancer patients (4, 7, 8). Under physiological conditions, the immune system is able to recognize genetically altered cancerous cells and eliminate them from our bodies. Thus, a functional immune surveillance system may explain why most people do not have a clinically manifested malignant disease (11).

A clinically detectable cancer mass represents the failure of immune surveillance to eliminate malignant cells. Several possible mechanisms may contribute to immune escape, including (i) genetic alterations of cancer cells to acquire immune tolerance; (ii) metabolic reprogramming of malignant cells; (iii) changes in the tumor microenvironment (TME); (iv) alterations of stromal cellular components; (v) production of immunosuppressive molecules to inactivate the immune surveillance functions; (vi) prevention of immune cell infiltration in tumors; and (vii) general dysfunctional immune response in cancer hosts. Accumulating preclinical and clinical evidence supports these mechanisms, which suggest that the development of novel therapeutics to target these pathways can improve the efficacy of cancer immunotherapies. For example, tumor cells frequently express high levels of immunosuppressive surface molecules, such as PD-L1, to paralyze the tumor-attacking ability of T lymphocytes (12, 13). Blocking these immunosuppressive molecules by immune checkpoint inhibitors, such as pembrolizumab, is now routinely used in patients (14). Similarly, blocking immunosuppressive receptors, such as PD-1 and CTLA-4, in T cells by nivolumab and ipilimumab also produces marked anticancer activity in cancer patients (15, 16). In addition, lymphocyte-based therapeutics, known as adoptive cell therapy, including tumor-infiltrating lymphocytes (TILs), natural killer cells, and chimeric antigen receptor T (CAR-T) cells, represent breakthroughs in cancer therapy over the last decade (7, 17, 18). Despite the clinical promise of immunotherapy, in most cancer types, only a minority of cancer patients benefit from these therapeutics.

Metastatic disease is the primary cause of mortality in most cancer patients (19). At the time of diagnosis, patients often experience metastatic disease via lymphatic or hematogenous routes. Metastasis can occur at the very early stage of cancer development when a primary tumor mass is still tiny. The metastatic cascade includes intravasation of cancer cells into the circulation, extravasation in a distal tissue or organ, formation of the initial metastatic niche, and regrowth of a metastatic nodule

Significance

The clinical efficacy of immunotherapy in cancer patients is limited. We have developed a zebrafish model that allows us to visualize the metastatic cancer cell-killing effect by tumor-infiltrating lymphocytes and chimeric antigen receptor T cells in vivo at the single-cell level. This in vivo model accurately predicts clinical efficacy of T cell-mediated cancer therapy. Our data provide an in vivo platform for validating antimetastatic effects by human T cell-mediated immunotherapy. Based on our findings, it is highly recommended that anticancer effects of T cells isolated from cancer patients or genetically propagated T cells should be evaluated in this in vivo animal model before clinical application. If so, millions of cancer patients might benefit from our work.

Author contributions: Y. Cao designed research; X.H., X.Y., J.W., Q.D., S.Q., X.J., K.H., J.W., L.D.J., and L.B. performed research; Y.D., Q.D., S.Q., S.Y., X.J., J.W., A.L., A.I.S., L.B., W.T., and Y. Chen participated in experimentation; S.L.W., Y.D., S.Y., A.L., A.I.S., W.T., Y. Chen, and R.K. contributed new reagents/analytic tools; X.H. and Y. Cao analyzed data; and Y. Cao wrote the paper.

The authors declare no competing interest.

This article is a PNAS Direct Submission.

[1]To whom correspondence may be addressed. Email: yihai.cao@ki.se.

This article contains supporting information online at https://www.pnas.org/lookup/suppl/doi:10.1073/pnas.2009092117/-/DCSupplemental.

First published August 28, 2020.

into a clinically detectable mass (20–22). Clinically detectable metastases represent the final stage of these complex processes (23). Currently, no imaging techniques are available to detect microscopic metastatic nodules in living human patients.

Our laboratory and others have developed a zebrafish metastasis model that allows us to study the metastatic process of human cancers at the single-cell level (22, 24–29). In particular, this unique model offers an opportunity to visualize the initial process of cancer metastasis when primary tumors are tiny, usually consisting of several hundreds of cells. Using a multiple color-coding system, we are able to reconstitute the TME in the immune-privileged and transparent zebrafish body (25, 26).

In this paper, we report our recent findings using the zebrafish metastasis model to study the cancer-killing effect of TILs and CAR-T cells. Both TILs and CAR-T cells recognize metastatic cancer cells and execute the killing effect. The highlights of the present work are as follows: (i) a visualized system to discriminate intact cancer cells from damaged cancer cells in vivo, which allows us to directly visualize T cell-mediated killing effects; (ii) a quantitative system in vivo to determine the T cell-mediated cancer killing effects in vivo; (iii) an imaging system to study specific T cell recognition of metastatic cancer cells, including circulating cancer cells and resident metastatic cancer cells, and eliminate these malignant cells; (iv) the role of cancer-associated fibroblasts in protecting cancer cells from T cell-mediated killing; and (v) information about the clinical relevance of our findings.

On the basis of our findings, we propose that the zebrafish provides an attractive in vivo model to evaluate the anticancer effect of immune cells before their application in human patients. In particular, this model can predict the antimetastatic effects in cases when metastatic cells are not clinically detectable.

Results

Monitoring Human T Cell-Mediated Tumor Cell-Killing Effect In Vitro. To directly visualize the T cell-mediated tumor cell-killing effect, we developed a visualization system in which tumor cells were intracellularly labeled with a fluorescent dye (Fig. 1*A*). Nonfluorescent calcein AM is a lipophilic compound that can be efficiently taken up by tumor cells (30). In living cells, nonfluorescent calcein AM is converted into green fluorescent calcein by intracellular esterase-mediated ester hydrolysis. Green fluorescent calcein is a hydrophilic compound that is retained intracellularly. Mechanical damage, cellular lysis, and cell death can release the fluorescent calcein to the extracellular compartment (Fig. 1*A*).

To test whether calcein-labeled fluorescent cancer cells can be recognized by cytotoxic T cells, we isolated TILs from human melanoma patients (31). Human primary melanoma cells (hPMCs) from the same patient were labeled with green fluorescent calcein and cocultured with autologous TILs. Alter a 4-h coincubation, the majority of fluorescent-positive melanoma cells were lysed by TILs (Fig. 1*B*). Quantification analysis showed that >80% of calcein-positive melanoma cells were lysed by TILs. In contrast, human peripheral blood mononuclear cells (PBMCs) isolated from healthy individuals completely lacked cancer cell-killing effects (Fig. 1*B*). To further validate this visualization system, we used a CAR-T cell–human Raji B cell lymphoma paired system in which CAR-T cells recognized the Raji cell surface CD19 (32). Similarly, CAR-T exhibited a marked killing effect on Raji B cell lymphoma cells (Fig. 1*C*). Conversely, non–CD19-recognizing control CAR-T cells (EGFRt-T) completely lacked a cancer-killing effect. These findings show that calcein labeling does not affect the cancer cell-killing capacity of TILs and CAR-T cells.

To further advance our visualization system, we labeled TILs and CAR-Ts with red fluorescent DiI dye and analyzed the T cell-mediated oncolysis via a coculturing system. As expected, Dil-TILs at a ratio of 1:1 effectively killed human melanoma cells after a 4-h incubation (Fig. 1 *D* and *F*). The total number of TILs remained unchanged after this killing (Fig. 1*G*). In contrast, coincubation of melanoma cells with nonspecific PBMCs did not produce any killing effect on melanoma cells (Fig. 1 *D* and *F*). Similar to the TIL-hPMC system, coincubation of DiI–CAR-T cells with calcein-Raji cells also produced a very potent oncolytic effect, and most cancer cells were eliminated by CAR-T cells after a 4-h incubation (Fig. 1 *E* and *F*). FACS analysis further validated the tumor cell-killing effect (Fig. 1*H*).

Visualization of TIL-Mediated Melanoma Killing In Vivo. Having developed a visualization system for the red DiI-T cell-mediated killing of green fluorescent calcein-labeled cancer cells, we next investigated the visualization of T cell-mediated killing in vivo. We used a zebrafish cancer model in which human cancer cells were implanted in transparent zebrafish. Our previous work showed that this model has several unique advantages, including (i) visualization of human cancer cells in the fish body at the single cell level; (ii) allowing for a quantitative study of primary tumor growth; (iii) reconstitution of the TME by labeling various cellular components with different colors; (iv) allowing for study of tumor neovascularization; and (v) investigation of cancer metastasis at the early stage of primary tumor formation.

In this zebrafish cancer model, the green fluorescent calcein-labeled cancer cells were implanted into the perivitelline space around the yolk sac, followed by injection of DiI-T cells into the same position (Fig. 2*A*). Implantation of hPMCs into the perivitelline space allowed the formation of a fluorescence-positive primary tumor mass (Fig. 2*B*). At 24-h postimplantation, fluorescence-positive hPMCs remained in the perivitelline space (Fig. 2*B*). Coimplantation of green hPMCs with Dil-red PBMCs did not affect the hPMC population (Fig. 2 *C* and *E*), indicating that no tumor cell killing occurred. In contrast, coimplantation of Dil-red TILs with hPMCs for 24 h resulted in near-complete elimination of hPMCs in the zebrafish body (Fig. 2 *D* and *E*). Despite the potent tumor killing effect, the total population of Dil-red TILs remained unchanged after tumor killing (Fig. 2*F*). These data show that Dil-red TILs effectively eradicate human melanoma cells in the living zebrafish body. The TIL-mediated tumor killing could be visualized at the single- cell level.

CAR-T-Mediated Lymphoma Oncolysis in Zebrafish. To validate the TIL-mediated anticancer effect, we performed similar experiments using the CAR-T–Raji lymphoma system. Similar to human melanoma, implantation of Raji cells into the perivitelline space resulted in the formation of a cluster of tumor cells without obvious metastatic spread (*SI Appendix*, Fig. S1*A*). Coimplantation of Raji lymphoma cells and control CAR-T cells (EGFRt-T) lacking CD19 recognition did not affect tumor cell survival (*SI Appendix*, Fig. S1 *B* and *D*). Likewise, control CAR-T cells remained unaltered after coincubation with Raji lymphoma cells (*SI Appendix*, Fig. S1*E*). In contrast, coimplantation of CD19 recognizing CAR-T cells with Raji lymphoma cells for 24 h resulted in elimination of most cancer cells without significant loss of CAR-T cells (*SI Appendix*, Fig. S1 *C* and *D*). These findings provide further evidence to support the effective cancer killing effect by specific cytotoxic T cells in our zebrafish-tumor model.

Elimination of Metastatic Melanoma Cells by TILs. Metastasis is the most common cause of cancer-related death. Clinically visible metastases represent the ultimate stage of cancer metastasis consisting of a large population of cancer cells. Our recent work showed that metastasis can occur at the very early stage of cancer development when a primary tumor at the microscopic size contains only several hundred cancer cells (24). Such microscopic cancer metastases cannot be detected by the most advanced imaging analysis in human patients and in mammalian cancer models. Our zebrafish model provides a unique opportunity to study and visualize microscopic metastasis at the single-cell level when metastatic nodules are tiny.

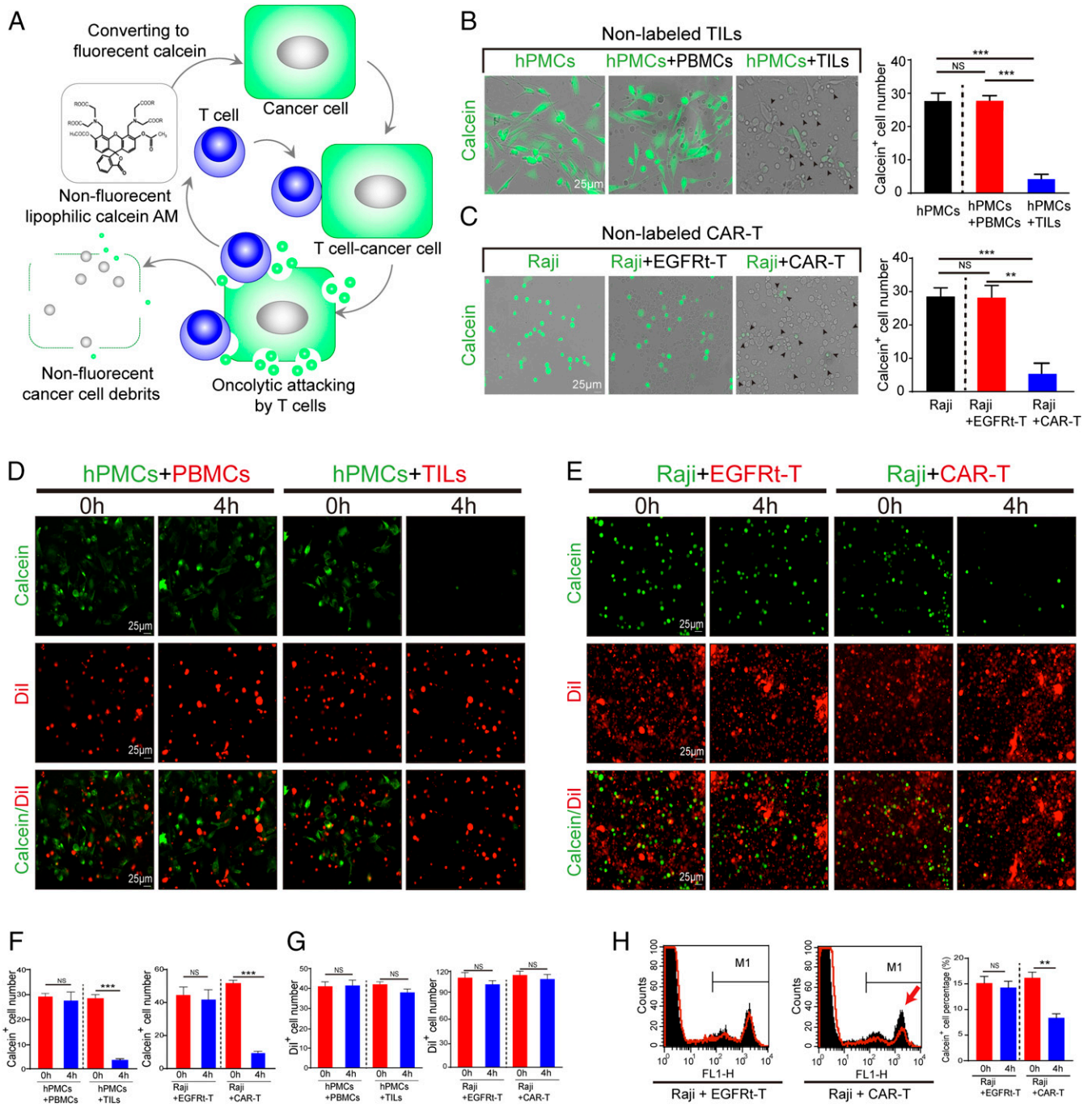

Fig. 1. Development of the color-coded system to monitor T cell-mediated cancer cell killing. (*A*) Calcein-based cancer cell labeling to discriminate living cells from dead cells. Hydrophobic nonfluorescent calcein AM is taken up by cancer cells and subsequently converted into green fluorescent hydrophilic calcein by intracellular esterase in living cells. Green fluorescent calcein is retained in the cytoplasm due to its hydrophilic properties. When tumor-specific T cells attack calcein-labeled cancer cells, the intracellular calcein is released to the extracellular space, and cancer cells become fluorescence-negative dead cells. (*B* and *C*) Micrographs of calcein-labeled hPMCs (green), hPMCs plus human PBMCs, hPMCs plus TILs, Raji lymphoma cells, Raji cells plus EGFRt–CAR-T cells, and Raji cells plus CD19–CAR-T cells. Cells were cultured for 4 h. Arrows indicate TIL- and CAR-T cell-lysed cancer cells. Calcein-positive hPMCs are quantified (n = 4 to 5 random fields [20×] per group). (Scale bar: 25 μm.) (*D* and *E*) Micrographs of calcein-labeled hPMCs (green), hPMCs plus DiI-labeled human PBMCs (red), green hPMCs plus DiI-labeled TILs (red), calcein-labeled Raji lymphoma cells (green), calcein-labeled Raji cells (green) plus DiI-labeled EGFRt–CAR-T cells (red), and calcein-labeled Raji cells (green) plus DiI-labeled CD19–CAR-T cells(red). Cells were cultured for 0 h and 4 h. (Scale bar: 25 μm.) (*F*) Quantification of calcein-positive hPMCs and Raji cells (n = 3 to 5 random fields [20×] per group). (*G*) Quantification of DiI-positive TILs, PBMCs, EGFRt–CAR-T, and CD19–CAR-T cells (n = 3 to 5 random fields [20×] per group). (*H*) FACS analysis of calcein-positive Raji cells after coculturing with CD19–CAR-T cells and EGFRt–CAR-T cells for 4 h. Living cells (M1 gate) represent the calcein-positive population. The red line indicates cell numbers after a 4-h coculture, and the black area indicates cell numbers after a 0-h coculture. Calcein-positive Raji cells are quantified. Data are mean ± SEM; n = 3 samples per group. $^{**}P < 0.01$; $^{***}P < 0.001$; NS, not significant, Student's t test.

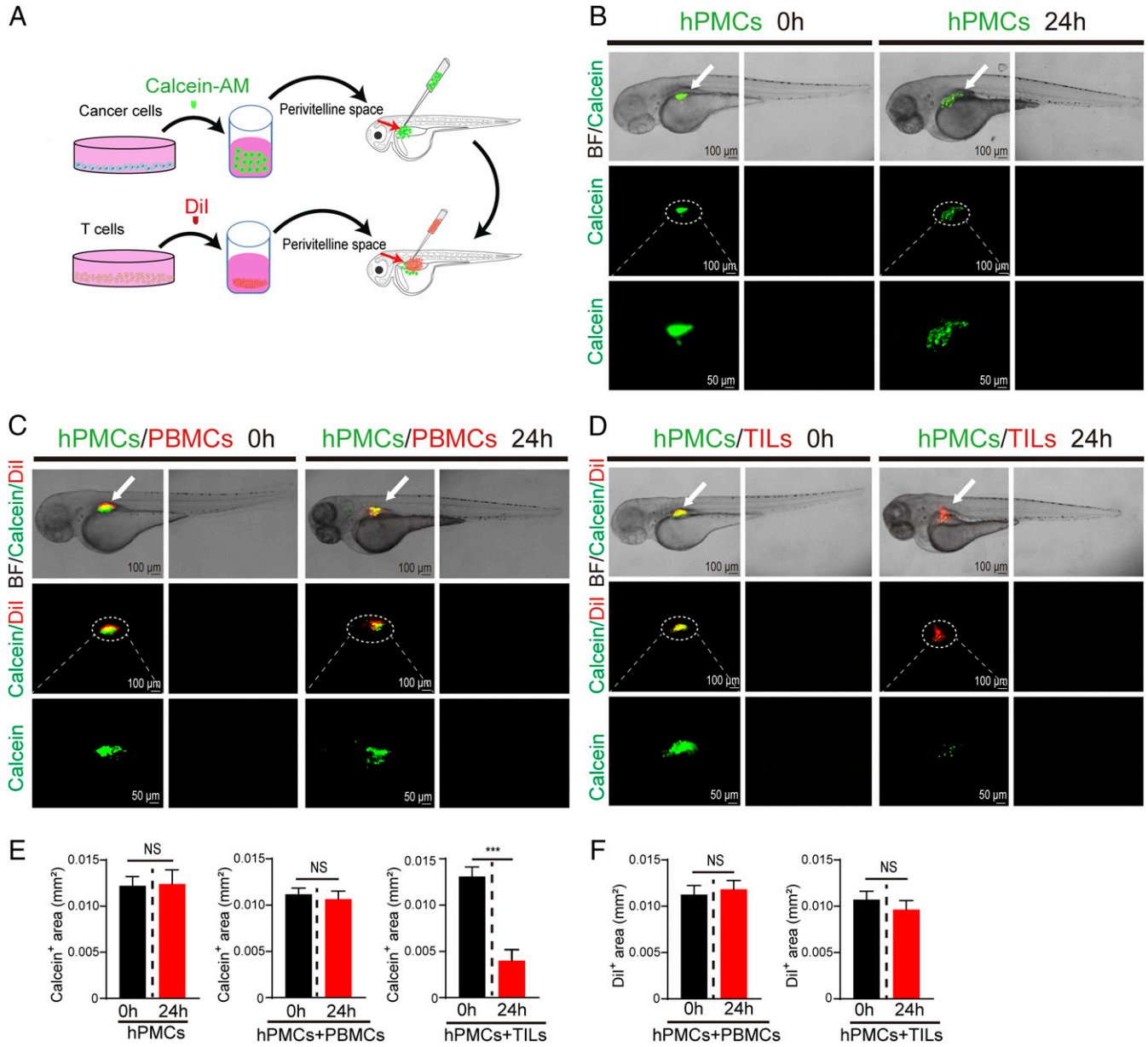

Fig. 2. Elimination of hPMCs by TILs in zebrafish. (*A*) Schematic diagram of the experimental design. Calcein-labeled cancer cells (green) were implanted into the perivitelline space of each zebrafish, and DiI-labeled T cells (red) were subsequently implanted into the same space in each zebrafish. The survival of cancer cells and T cells was monitored. (*B–D*) Micrographs of zebrafish bearing hPMCs alone (green), hPMCs (green) plus PBMCs (red), and hPMCs (green) plus TILs (red). At 24 h postimplantation, survival rates of cancer cells and T cells were analyzed. Arrows indicate primary tumor sites. Dashed lines circle and amplify the indicated regions. (Scale bars: 100 μm; in amplified fields, 50 μm.) (*E* and *F*) Quantification of calcein-positive (green) and DiI-positive (red) areas in the zebrafish (hPMCs alone, $n = 15$ samples per group; hPMCs plus PBMCs, $n = 24$ samples per group; hPMCs plus TILs, $n = 24$ samples per group). Data are mean ± SEM. ***$P < 0.001$; NS, not significant, paired-sample t test.

To study the metastatic killing effect by T cells, tumor cells were implanted into the common cardinal vein (CCV, or the duct of Cuvier) to establish an experimental metastasis model (Fig. 3*A*). Following tumor cell implantation, cancer-attacking lymphocytes are implanted into the same site. As shown in Fig. 3*B*, injection of human melanoma cells into the CCV resulted in rapid spread of cancer cells in the zebrafish body (Fig. 3*B*). In particular, calcein-fluorescent single melanoma cells could be clearly visualized in the trunk and tail parts of the zebrafish body. Coimplantation of hPMCs and control PBMCs did not affect the metastatic melanoma cell population (Fig. 3 *C* and *E*). Both calcein-labeled green hPMCs and DiI-labeled PBMCs were evident in the zebrafish body (Fig. 3*C*). Intriguingly, CCV coimplantation of hPMCs and TILs eradicated the majority of metastatic cancer cells (Fig. 3 *D*, *E*, and *G*). The number of the invested DiI-labeled TILs in the head and tail regions was slightly increased (Fig. 3*F* and *SI Appendix*, Fig. S2*A*). These findings show that TILs effectively eliminate circulating cancer cells in the zebrafish body.

Eradication of Metastatic Cancer Cells by CAR-T Cells. We next studied the impact of CAR-T cells on the killing of metastatic cancer cells in the living zebrafish body. CCV injection of human lymphoma cells also resulted in widespread distribution of cancer cells in the zebrafish body (Fig. 4*A*). Coimplantation of control CAR-T cells (EGFRt-T) had no effect on metastatic cancer cells (Fig. 4 *B* and *D*). In contrast, CD19-recognizing

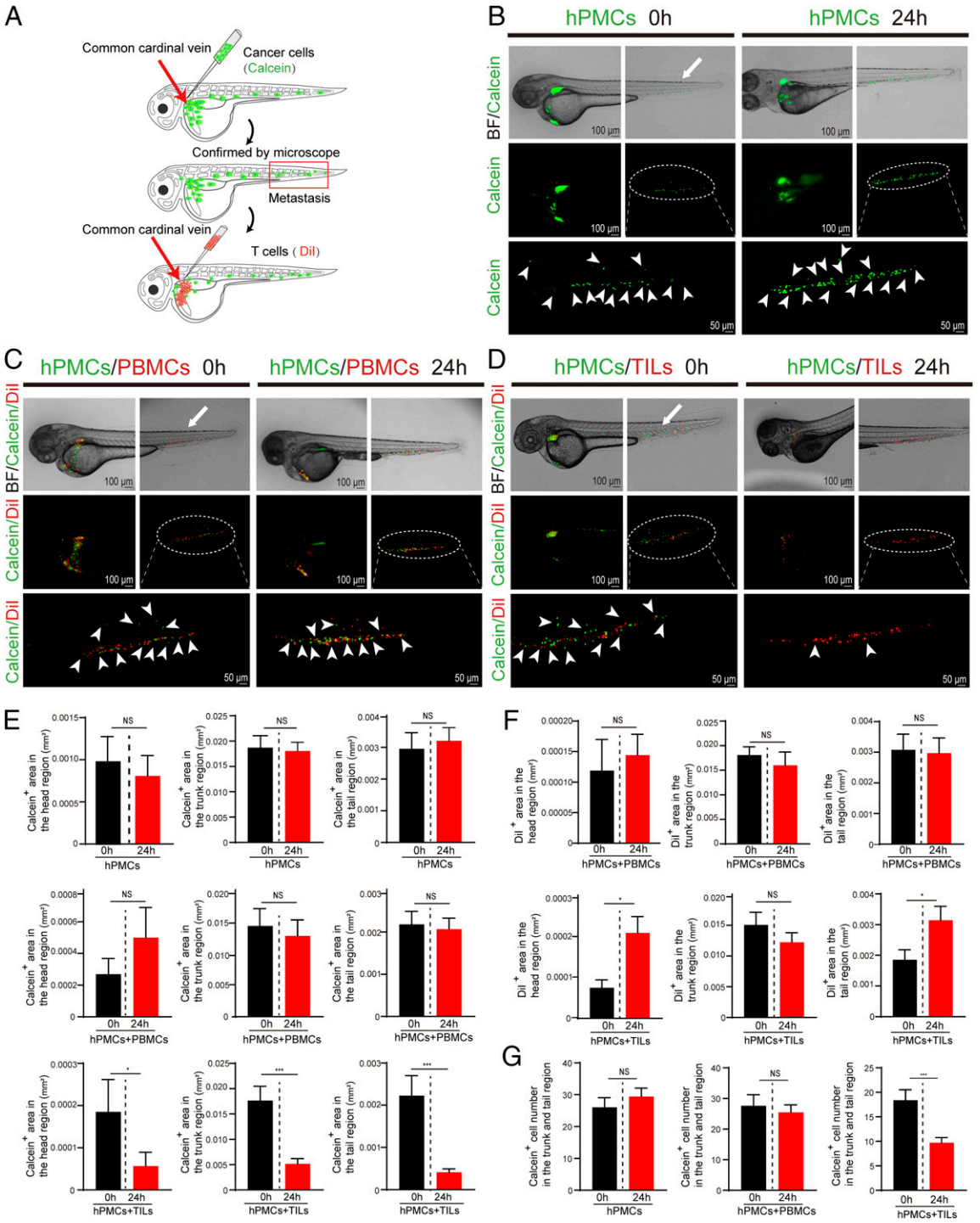

Fig. 3. Eradication of metastatic cancer cells by T cells in zebrafish. (*A*) Metastatic model in zebrafish. Calcein-labeled cancer cells (green) were injected into the CCV of each zebrafish to induce widespread cancer metastasis in the zebrafish body. Metastatic foci (green) in distal regions, including the trunk-tail part of each zebrafish, were readily visualized by fluorescence microscopy examination. After metastatic validation, DiI-labeled T cells (red) were subsequently injected into the CCV of recruited zebrafish. Survival rates of cancer cells and T cells in the head, trunk, and tail regions of zebrafish were examined under a fluorescent microscope. (*B*) Metastatic spread of calcein-labeled hPMCs (green) in zebrafish after 0-h and 24-h CCV implantation of cancer cells. The arrow indicates visible metastatic cancer cells. Dashed lines encircle metastatic cancer cells in the trunk-tail region of the zebrafish body. Arrowheads indicate metastatic cancer cells. (Scale bars: 100 μm; in amplified fields, 50 μm.) (*C* and *D*) Metastatic cancer cells in hPMCs (green) plus PBMCs (red) and hPMCs (green) plus TILs (red) at 0 h and 24 h after CCV implantation. The arrow indicates visible metastatic cancer cells. Dashed lines encircle metastatic cancer cells in the trunk-tail region of the zebrafish body. Arrowheads indicate metastatic cancer cells. (Scale bars: 100 μm; in amplified fields, 50 μm.) (*E*) Quantification of calcein (green)-positive areas of melanoma cells in the head, trunk, and tail regions of zebrafish (hPMCs alone, $n = 13$ samples per group; hPMCs plus PBMCs, $n = 15$ samples per group; hPMCs plus TILs, $n = 29$ samples per group). (*F*) Quantification of DiI (red)-positive areas of PBMCs and TILs in the head, trunk, and tail regions of zebrafish (hPMCs plus PBMCs, $n = 15$ samples per group; hPMCs plus TILs, $n = 29$ samples per group). (*G*) Quantification of calcein (green)-positive melanoma cells in the trunk and tail regions of zebrafish (hPMCs alone, $n = 13$ samples per group; hPMCs plus PBMCs, $n = 15$ samples per group; hPMCs plus TILs, $n = 29$ samples per group). Data are mean ± SEM. $^*P < 0.05$; $^{***}P < 0.001$; NS, not significant, paired-sample *t* test.

CAR-T cells eradicated the majority of metastatic cancer cells (Fig. 4 *C*, *D*, and *F*). After a 24-h incubation, the number of the invested DiI-labeled CAR-T cells did not change significantly (Fig. 4*E* and *SI Appendix*, Fig. S2*B*). These data demonstrate that CD19 CAR-T cells specifically recognize lymphoma cells in the fish body and perform specific killing.

It should be emphasized that despite potent eradication of cancer cells, the zebrafish remained completely healthy and indistinguishable from control zebrafish. Zebrafish viability and behavior were completely unaffected in the CAR-T lymphoma-implanted zebrafish embryos, verifying the specific cancer cell-killing effect with no effect on other cells.

Protection of Metastatic Cancer Cells from T Cell-Mediated Killing by CAFs. In the TME, malignant cells communicate with other stromal cells to collectively influence tumor growth, metastasis, and drug responses. In particular, stromal fibroblasts, also known as named cancer-associated fibroblasts (CAFs), play an important role in modulating tumor growth and metastasis (33). Our recent work shows that CAFs and cancer cells can form clusters in the zebrafish (25); however, whether CAFs can significantly affect the T cell-mediated killing effect on cancer cells is unknown. To explore this, human CAFs were isolated from colorectal cancer tissues, mixed with hPMCs, and subsequently implanted into the perivitelline space (Fig. 5 *A* and *B*).

In contrast to eradication of hPMCs by TILs (Fig. 5 *C* and *E*), CAFs nearly completely protected hPMCs from the TIL-executed killing (Fig. 5 *D* and *E*). In CAF and hPMC-coimplanted zebrafish, the number of DiI-labeled TILs remained unchanged after a 24-h incubation with TILs (Fig. 5*F*). Similar protective effects of CAFs were also seen with the CAR-T–Raji paired system (*SI Appendix*, Fig. S3). These data indicate that CAFs protect melanoma cells from T cell-mediated killing.

CCV injection of CFAs and hPMCs resulted in widespread distribution of metastatic cancer cells in the bloodstream (Fig. 6). Interestingly, most metastatic hPMCs were physically coupled with CAFs to form metastatic hPMC-CAF cell clusters (Fig. 6 *B*–*F*). These findings support our previously published findings that cancer cells and CAFs co-metastasize in the bloodstream (25). Notably, CAFs significantly neutralized the TIL-mediated killing effects on cancer cells at 24 h postimplantation, leading to markedly protective effects that were indistinguishable from the initial invested cell numbers (Fig. 6). Again, CAF-mediated protective effects were also seen using the CAR-T–Raji system (*SI Appendix*, Fig. S4). These findings provide convincing evidence that CAFs protect cancer cells from T cell-executed killing.

Discussion

Removal of metastatic cells in cancer patients is probably the most important approach in cancer therapy. Elimination of clinically undetectable microscopic metastases that consist of only a few hundred, thousand, or even greater numbers of cells could provide a curative therapy. Surgery and radiation therapy offer local therapeutic approaches for treating clinically visible primary and metastatic tumor masses. Although the systemic delivery of chemotherapeutics has some impact on metastatic cancer cells, these drugs target only the proliferative population of cancer cells. Metastatic recurrence often happens months to years after removal of the primary tumor mass (34–36). After resettling in distal organs, metastatic cancer cells usually remain dormant without further proliferation (37), posing a difficult problem for cancer therapy because most anticancer drugs have no impact on these dormant cancer cells. Owing to the intrinsic property of genomic instability inherited from their primary tumors, dormant metastatic cancer cells may undergo relentless genetic mutations, triggering additional signaling activation of regrowth. Indeed, genetic alterations of metastatic cancer cells often differ from their primary cancer cells (38).

How do we identify these dormant metastatic cancer cells and eradicate them? Targeted therapeutics may play certain roles in eliminating metastatic cancer cells; however, owing to the heterogeneity of cancer cell populations, targeted therapeutics may eradicate only a subpopulation of cancer cells and leave other malignant cells untouched. Immunotherapy heralds an exciting era for curative treatment of cancers. Enhancing cancer cell recognition via antibody-induced activation of endogenous cytotoxic T cells and administration of exogenously educated and engineered T cells has proven remarkably beneficial for cancer patients (1, 6, 7, 14–16, 38). However, for most cancer types, immunotherapy is beneficial for only a minority of patients. This limited therapeutic outcome makes it essential to discriminate responders from nonresponders. To achieve this goal, appropriate, reliable in vivo preclinical models are needed to recapitulate the patient situation. Unlike cancer models in rodents, our zebrafish cancer model provides a unique opportunity to study T cell-mediated cancer killing. Specific features include (i) transparent visualization of interaction between T cells and cancer cells in the living body; (ii) implantation of human primary cancer cells and T cells in immune-privileged zebrafish embryos; (iii) color-coding of human T cells and cancer cells; (iv) distinction of living cancer cells from oncolytically dead cells at the single cell level; (v) tracing of single metastatic cancer cells in the living body; (vi) visualization of T cell-mediated eradication of metastatic cancer cells; (vii) need for a minimal number of cells; and (viii) elucidation of the impact of tumor stromal cells on T cell-mediated cancer cell killing.

In this study, we have further advanced the zebrafish cancer model by visualizing the oncolytic process of lymphocytes. The colorful calcein is a hydrophilic molecule and remains intracellularly. On specific T cell attacks, green calcein in cancer cells is released to the extracellular space. In zebrafish, this system dictates the specific T cell-mediated cancer killing, which is reliable and reminiscent of the clinical scenario.

One of the most important aspects of our work is the visualization of metastatic cancer killing by T cells. Cancer-killing specific T cells are able to identify distal metastatic cancer cells and eliminate them. Since the implanted cancer cells in the zebrafish body are quiescent, our data indicate that TILs and CAR-T cells recognize potentially dormant cancer cells to execute the killing effect. These findings are extremely exciting and clinically significant. If they can be successfully translated into the clinical setting, TILs and CAR-T cells will be able to eliminate microscopically dormant cancer cells to achieve a cure. An extension of this clinical implication would be administration of TILs and CAR-T cells to cancer patients after removal and destruction of primary tumors. This sequential therapeutic regimen would allow extinction of residual cancer cells surrounding the primary site and in distal organs. Moreover, our study also supports the ability of TILs and CAR-T cells to effectively eliminate circulating cancer cells in the bloodstream. Therefore, some combination of conventional therapy and T cell-based immunotherapy might offer a curative approach for treating cancers. Although we use melanoma and lymphoma as examples, our findings can be reasonably extended to other types of cancers as well.

Another potential clinical implication of our zebrafish model is the ability to assess the efficiency of cancer cell killing by specific T cells. Since most cancer patients do not benefit from immunotherapy, a reliable and simple preclinical model is needed to assess the cancer-killing effect, and the zebrafish model would be an ideal model for this purpose. The model is simple, and the results can be reliably reported after an experiment of 24 h. Furthermore, as shown in the present study only several hundred cells are sufficient for implantation into each zebrafish. Thus, clinical samples from biopsies would be sufficient to perform functional experiments in the zebrafish body.

Although the concept has not been experimentally approved, we expect that our zebrafish model will provide a unique platform on which to test the anticancer effects of immunotherapy in combination with other targeted therapeutics. In particular, blocking cancer inflammation and fibrosis may further enhance the therapeutic efficacy of immunotherapy. Taken together, our

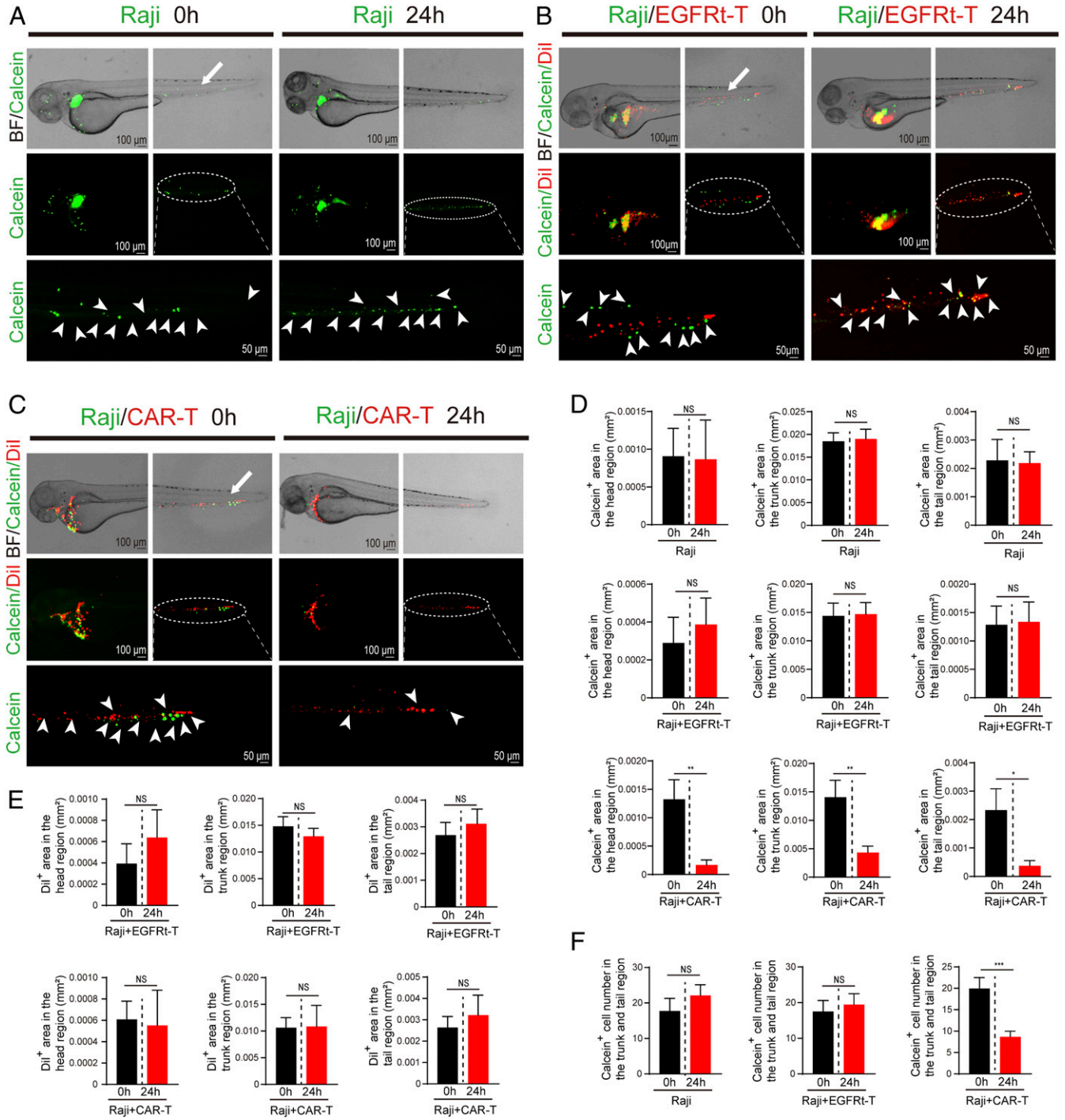

Fig. 4. Eradication of metastatic Raji cells by CAR-T cells in zebrafish. (*A*) Metastatic spread of calcein-labeled Raji cells (green) in zebrafish at 0 h and 24 h after CCV implantation of cancer cells. The arrow indicates visible metastatic cancer cells. Dashed lines encircle metastatic cancer cells in the trunk-tail region of the zebrafish body. Arrowheads indicate metastatic cancer cells. (Scale bars: 100 μm; in amplified fields, 50 μm.) (*B* and *C*) Metastatic cancer cells of Raji cells (green) plus EGFRt–CAR-T cells (red) and Raji cells (green) plus CD19–CAR-T cells (red) at 0 h and 24 h after CCV implantation. The arrow indicates visible metastatic cancer cells. Dashed lines encircle metastatic cancer cells in the trunk-tail region of the zebrafish body. Arrowheads indicate metastatic cancer cells. (Scale bars: 100 μm; in amplified fields, 50 μm. (*D*) Quantification of calcein (green) positive area of Raji cells in the head, trunk, and tail regions of zebrafish. (Raji cells alone, $n = 15$ samples per group; Raji cells plus EGFRt–CAR-T cells, $n = 15$ samples per group; Raji cells plus CD19–CAR-T cells, $n = 15$ samples per group). (*E*) Quantification of DiI (red)-positive areas of EGFRt–CAR-T cells and CD19–CAR-T cells (Raji cells plus EGFRt–CAR-T cells, $n = 15$ samples per group; Raji cells plus CD19–CAR-T cells, $n = 15$ samples per group). (*F*) Quantification of calcein (green)-positive Raji cells in the trunk and tail regions of zebrafish (Raji cells alone, $n = 15$ samples per group; Raji cells plus EGFRt–CAR-T cells, $n = 15$ samples per group; Raji cells plus CD19–CAR-T cells, $n = 15$ samples per group). Data are mean ± SEM. $^*P < 0.05$; $^{**}P < 0.01$,$^{***}P < 0.001$; NS, not significant, paired-samples *t* test.

experimental data demonstrate that a zebrafish cancer model has tremendous clinical implications for determining the therapeutic efficacy of immunotherapy in treating primary and metastatic cancers.

Materials and Methods

Cell Source and Culture. Raji cells, $CD8^+$-CD19 CAR-T cells, and EGFRt-T-cells were grown in 10% FBS-RPMI 1640 medium (Life Technologies). Human

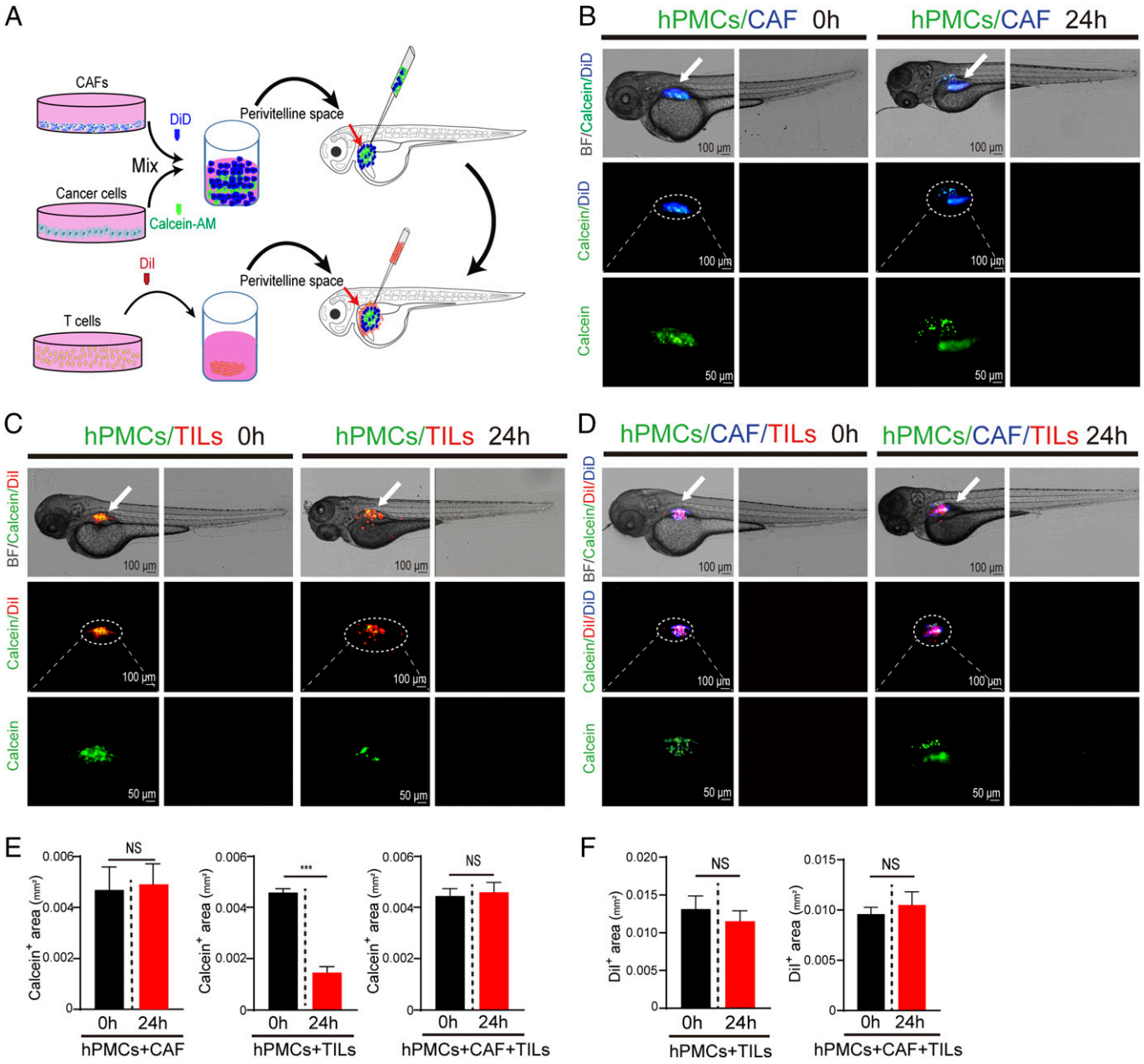

Fig. 5. CAFs protect primary tumors from T cell-mediated killing. (*A*) Isolated human primary CAF cells labeled with DiD (blue) were isolated from human colorectal cancers. CAFs (blue) and calcein-labeled hPMCs (green) at the ratio of 2:1 were mixed and subsequently coimplanted into the perivitelline space of each zebrafish. The same number of DiI-labeled TILs (1:1 hPMCs and TILs) (red) were implanted into the same location. TIL-executed cancer cell killing was analyzed at 24 h after TIL implantation. (*B*) CAFs (blue) and hPMCs (green) at 0 h and 24 h after coimplantation. The arrows indicate the primary tumor sites. Dashed lines encircle primary tumors in the perivitelline space. (Scale bars: 100 μm; in amplified fields, 50 μm. (*C* and *D*) Representative micrographs of hPMCs (green) plus TILs (red), hPMCs (green)/CAF (blue)/TILs (red) at 0 h and 24 h after coimplantation. Dashed lines encircle primary tumors in the perivitelline space. (Scale bars: 100 μm; in amplified fields, 50 μm.) (*E* and *F*) Quantification of calcein (green)- and DiI (red)-positive areas in the zebrafish (hPMCs plus CAF, $n = 6$ samples per group; hPMCs plus TILs, $n = 7$ samples per group; hPMCs/CAF/PBMCs, $n = 10$ samples per group). Data are mean ± SEM. ***$P < 0.001$; NS = not significant, paired-samples t test.

primary melanoma cells and CAFs were grown in 20% FBS-Iscove's modified Dulbecco's medium. More detailed information is provided in *SI Appendix, Materials and Methods*.

Isolation of Human Primary Melanoma Cells and TILs. Primary melanoma cells were isolated from a tumor tissue sample obtained from a patient diagnosed with stage IV melanoma (acronym MAT02 p11). The protocol for patient participation was approved by the local Ethics Committee (2013/516–31/1 and 2016/2123) and the Karolinska Institute's Institutional Review Board. All patients signed a written informed consent in accordance with the Declaration of Helsinki.

Tumor tissues were resected by mechanical separation, and tumor cells were cultured in RPMI-1640 supplemented with FCS (20%), penicillin (100 U/mL; Life Technologies), and streptomycin (100 μg/mL; Life Technologies). Tumor cells were frequently monitored for growth and medium was changed/cultures expanded when needed. TILs were expanded as described previously (39). In brief, TILs were expanded by stimulating tumor fragments with IL-2 alone and then performing a rapid expansion protocol via stimulation with IL-2 and anti-CD3 antibodies in the presence of irradiated PBMCs as feeder cells in RPMI-1640 supplemented with 1% to 10% human AB serum.

Zebrafish Tumor Model. All zebrafish work was performed in accordance with regulations of the Karolinska Institutet's Zebrafish Core Facility. The viability of T cell tumor-implanted zebrafish was determined by assessing heartbeat,

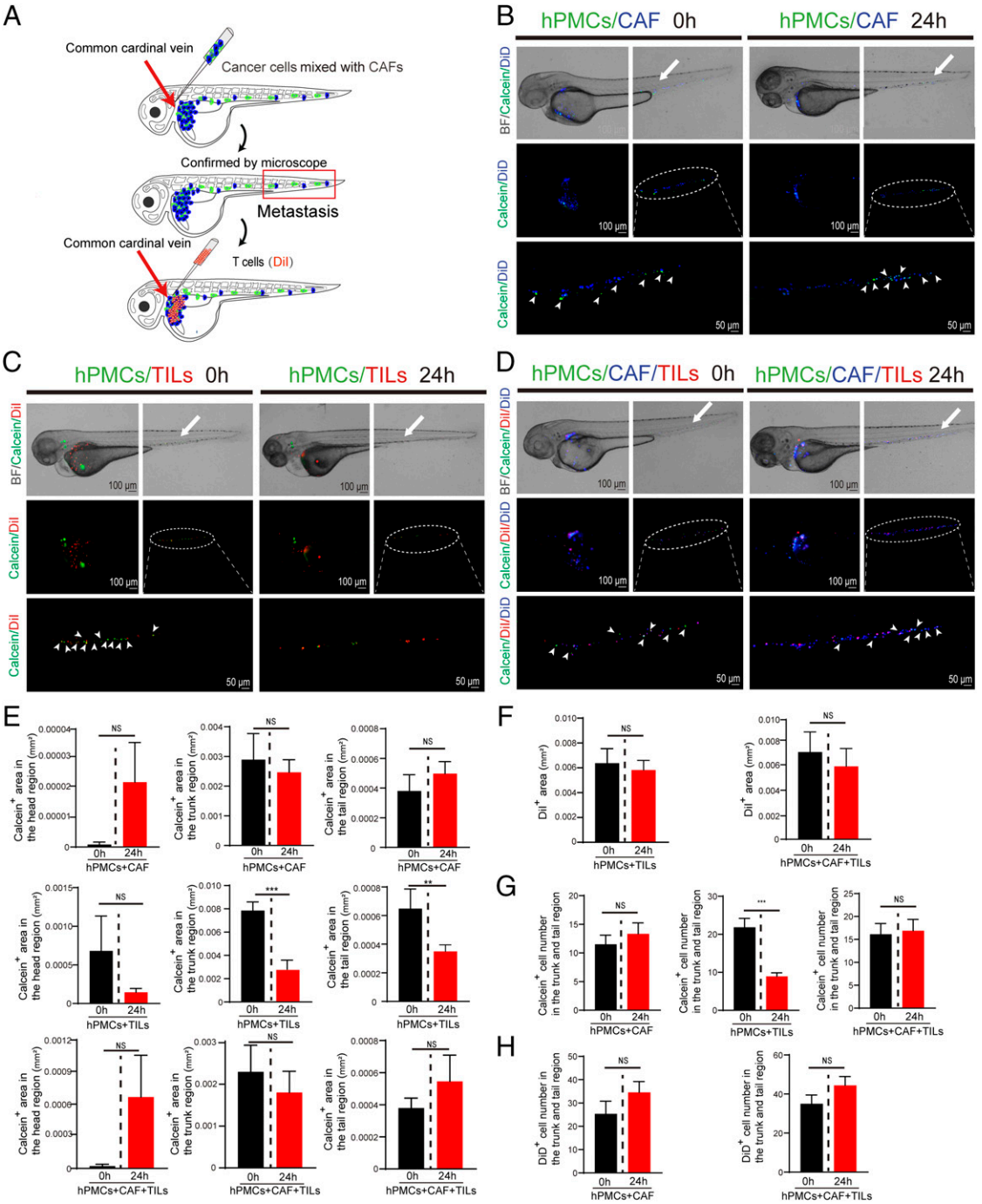

Fig. 6. CAFs protect metastatic cancer cells from T cell-mediated killing. (*A*) Isolated human primary CAF cells labeled with DiD (blue) were isolated from human colorectal cancers. CAFs (blue) and calcein-labeled hPMCs (green) at a ratio of 2:1 were mixed and subsequently coimplanted into the CCV of each zebrafish to induce widespread cancer metastasis in the zebrafish body. Metastatic foci (green) in distal regions including the truck-tail part of each zebrafish were readily visualized by fluorescence microscopy examination. After metastatic validation, the same number of DiI-labeled TILs (1:1 hPMCs and TILs) (red) were subsequently injected into the CCV of recruited zebrafish. Survival rates of cancer cells and T cells in the head, trunk, and tail regions of zebrafish were examined under a fluorescent microscope. (*B*) Metastatic spread of CAFs (blue) and hPMCs (green) at 0 h and 24 h after CCV coimplantation. The arrow indicates visible metastatic cancer cells. Dashed lines encircle metastatic cancer cells in the trunk-tail region of the zebrafish body. Arrowheads indicate metastatic cancer cells. (Scale bars: 100 μm; in amplified fields, 50 μm.) (*C* and *D*) Representative micrographs of hPMCs (green) plus TILs (red), hPMCs (green)/CAF (blue)/TILs (red) at 0 h and 24 h after CCV coimplantation. The arrow indicates visible metastatic cancer cells. Dashed lines encircle metastatic cancer cells in the trunk-tail region of the zebrafish body. Arrowheads indicate metastatic cancer cells. (Scale bars: 100 μm; in amplified fields, 50 μm.) (*E*) Quantification of calcein (green)-positive areas of melanoma cells in the head, trunk, and tail regions of zebrafish (hPMCs plus CAF, $n = 6$ samples per group; hPMCs plus TILs, $n = 13$ samples per group; hPMCs/CAF/TILs, $n = 9$ samples per group). (*F*) Quantification of DiI (red)-positive areas of TILs in the zebrafish (hPMCs plus TILs, $n = 13$ samples per group; hPMCs/CAF/TILs, $n = 9$ samples per group). (*G*) Quantification of calcein (green)-positive melanoma cells in the trunk and tail regions of zebrafish (hPMCs plus CAF, $n = 6$ samples per group; hPMCs plus TILs, $n = 13$ samples per group; hPMCs/CAF/TILs, $n = 9$ samples per group). (*H*) Quantification of DiD (blue)-positive CAF numbers in the trunk and tail regions of zebrafish (hPMCs plus CAF, $n = 6$ samples per group; hPMCs/CAF/TILs, $n = 9$ samples per group). Data are mean ± SEM. $^{**}P < 0.01$; $^{***}P < 0.001$; NS, not significant, paired-samples *t* test.

blood circulation, and physical movement. More details are provided in *SI Appendix, Materials and Methods*.

Flow Cytometry Based Calcein Retention Assay. Calcein-labeled Raji cells were transferred to each tube for flow cytometry, and data were analyzed using BD CellQuest Pro. See *SI Appendix, Materials and Methods* for details.

Fluorescence Analysis. Harvested CAR-T cells, TILs, and tumor cells were analyzed under a fluorescent microscope (Nikon Eclipse C1), randomized images were captured, and data were analyzed using ImageJ software. More details are provided in *SI Appendix, Materials and Methods*

Statistical Analysis. Statistical analysis was performed using the standard Student *t* test or paired-sample *t* test. Data are presented as mean of determinants (SEM), and the following *P* values were considered significant: $*P < 0.05$; $**P < 0.01$; $***P < 0.001$.

Data Availability. All study data are included in the main text and *SI Appendix*.

ACKNOWLEDGMENTS. The Y. Cao laboratory is supported by research grants from the European Research Council (ERC) advanced grant ANGIOFAT (Project 250021), the Swedish Research Council, the Swedish Cancer Foundation, the Swedish Children's Cancer Foundation, the Karolinska Institute Foundation, the Karolinska Institute's Distinguished Professor Award, the Torsten Söderberg Foundation, the Strategic Research Areas (SFO)-Stem Cell and Regeneration Medicine Foundation the Karolinska Institute, the Maud and Birger Gustavsson Foundation, a NOVO Nordisk Foundation advance grant, the NOVO Nordisk Foundation, and the Knut and Alice Wallenberg Foundation. The R.K. laboratory is supported by grants from the Swedish Cancer Society CAN2016/315, the Cancer Society in Stockholm 164073, the Swedish Medical Research Council 2016-01414, Stockholm City Council Project Grant 201700452, and the "Knut and Alice Wallenberg Foundation" (KAW2015.0063).

1. A. Ribas, Tumor immunotherapy directed at PD-1. *N. Engl. J. Med.* **366**, 2517–2519 (2012).
2. S. M. Ansell *et al*., PD-1 blockade with nivolumab in relapsed or refractory Hodgkin's lymphoma. *N. Engl. J. Med.* **372**, 311–319 (2015).
3. A. Snyder *et al*., Genetic basis for clinical response to CTLA-4 blockade in melanoma. *N. Engl. J. Med.* **371**, 2189–2199 (2014).
4. M. M. Gubin *et al*., Checkpoint blockade cancer immunotherapy targets tumour-specific mutant antigens. *Nature* **515**, 577–581 (2014).
5. J. Wolchok, Putting the immunologic brakes on cancer. *Cell* **175**, 1452–1454 (2018).
6. W. A. Lim, C. H. June, The principles of engineering immune cells to treat cancer. *Cell* **168**, 724–740 (2017).
7. E. Tran, D. L. Longo, W. J. Urba, A milestone for CAR T cells. *N. Engl. J. Med.* **377**, 2593–2596 (2017).
8. L. Rosenbaum, Tragedy, perseverance, and chance: The story of CAR-T therapy. *N. Engl. J. Med.* **377**, 1313–1315 (2017).
9. M. Sasaki *et al*., Propranolol exhibits activity against hemangiomas independent of beta blockade. *NPJ Precis. Oncol.* **3**, 27 (2019).
10. J. L. Arbiser, M. Y. Bonner, L. C. Gilbert, Targeting the duality of cancer. *NPJ Precis. Oncol.* **1**, 23 (2017).
11. L. Zitvogel *et al*., The anticancer immune response: Indispensable for therapeutic success? *J. Clin. Invest.* **118**, 1991–2001 (2008).
12. H. Dong, G. Zhu, K. Tamada, L. Chen, B7-H1, a third member of the B7 family, co-stimulates T-cell proliferation and interleukin-10 secretion. *Nat. Med.* **5**, 1365–1369 (1999).
13. G. J. Freeman *et al*., Engagement of the PD-1 immunoinhibitory receptor by a novel B7 family member leads to negative regulation of lymphocyte activation. *J. Exp. Med.* **192**, 1027–1034 (2000).
14. E. B. Garon *et al*.; KEYNOTE-001 Investigators, Pembrolizumab for the treatment of non-small-cell lung cancer. *N. Engl. J. Med.* **372**, 2018–2028 (2015).
15. J. D. Wolchok *et al*., Nivolumab plus ipilimumab in advanced melanoma. *N. Engl. J. Med.* **369**, 122–133 (2013).
16. F. S. Hodi *et al*., Improved survival with ipilimumab in patients with metastatic melanoma. *N. Engl. J. Med.* **363**, 711–723 (2010).
17. S. A. Rosenberg *et al*., Use of tumor-infiltrating lymphocytes and interleukin-2 in the immunotherapy of patients with metastatic melanoma. A preliminary report. *N. Engl. J. Med.* **319**, 1676–1680 (1988).
18. P. Hari, R. V. Raj, H. Olteanu, Targeting CD38 in refractory extranodal natural killer cell-T-cell lymphoma. *N. Engl. J. Med.* **375**, 1501–1502 (2016).
19. D. Hanahan, R. A. Weinberg, Hallmarks of cancer: The next generation. *Cell* **144**, 646–674 (2011).
20. S. Valastyan, R. A. Weinberg, Tumor metastasis: Molecular insights and evolving paradigms. *Cell* **147**, 275–292 (2011).
21. P. Rouhi *et al*., Pathological angiogenesis facilitates tumor cell dissemination and metastasis. *Cell Cycle* **9**, 913–917 (2010).
22. S. L. Lee *et al*., Hypoxia-induced pathological angiogenesis mediates tumor cell dissemination, invasion, and metastasis in a zebrafish tumor model. *Proc. Natl. Acad. Sci. U.S.A.* **106**, 19485–19490 (2009).
23. C. Pan *et al*., Deep learning reveals cancer metastasis and therapeutic antibody targeting in the entire body. *Cell* **179**, 1661–1676.e19 (2019).
24. P. Rouhi *et al*., Hypoxia-induced metastasis model in embryonic zebrafish. *Nat. Protoc.* **5**, 1911–1918 (2010).
25. C. Liu *et al*., A zebrafish model discovers a novel mechanism of stromal fibroblast-mediated cancer metastasis. *Clin. Cancer Res.* **23**, 4769–4779 (2017).
26. J. Wang *et al*., Novel mechanism of macrophage-mediated metastasis revealed in a zebrafish model of tumor development. *Cancer Res.* **75**, 306–315 (2015).
27. I. J. Marques *et al*., Metastatic behaviour of primary human tumours in a zebrafish xenotransplantation model. *BMC Cancer* **9**, 128 (2009).
28. R. Fior *et al*., Single-cell functional and chemosensitive profiling of combinatorial colorectal therapy in zebrafish xenografts. *Proc. Natl. Acad. Sci. U.S.A.* **114**, E8234–E8243 (2017).
29. M. Fazio, J. Ablain, Y. Chuan, D. M. Langenau, L. I. Zon, Zebrafish patient avatars in cancer biology and precision cancer therapy. *Nat. Rev. Cancer* **20**, 263–273 (2020).
30. X. M. Wang *et al*., A new microcellular cytotoxicity test based on calcein AM release. *Hum. Immunol.* **37**, 264–270 (1993).
31. S. Wickström, T. Lövgren, Expansion of tumor-infiltrating lymphocytes from melanoma tumors. *Methods Mol. Biol.* **1913**, 105–118 (2019).
32. D. Sommermeyer *et al*., Fully human CD19-specific chimeric antigen receptors for T-cell therapy. *Leukemia* **31**, 2191–2199 (2017).
33. R. Kalluri, The biology and function of fibroblasts in cancer. *Nat. Rev. Cancer* **16**, 582–598 (2016).
34. U. Veronesi *et al*., Local recurrences and distant metastases after conservative breast cancer treatments: Partly independent events. *J. Natl. Cancer Inst.* **87**, 19–27 (1995).
35. G. N. Naumov, J. Folkman, O. Straume, L. A. Akslen, Tumor-vascular interactions and tumor dormancy. *APMIS* **116**, 569–585 (2008).
36. Y. Cao, Opinion: Emerging mechanisms of tumour lymphangiogenesis and lymphatic metastasis. *Nat. Rev. Cancer* **5**, 735–743 (2005).
37. L. Holmgren, M. S. O'Reilly, J. Folkman, Dormancy of micrometastases: Balanced proliferation and apoptosis in the presence of angiogenesis suppression. *Nat. Med.* **1**, 149–153 (1995).
38. M. Arnedos *et al*., Precision medicine for metastatic breast cancer—limitations and solutions. *Nat. Rev. Clin. Oncol.* **12**, 693–704 (2015).
39. I. Poschke *et al*., A phase I clinical trial combining dendritic cell vaccination with adoptive T cell transfer in patients with stage IV melanoma. *Cancer Immunol. Immunother.* **63**, 1061–1071 (2014).